ELSEVIER

Journal of Organometallic Chemistry 566 (1998) 45–59

Journal of Organometallic Chemistry

Matrix isolation infrared and density functional theoretical studies of organic silanones, $(CH_3O)_2Si{=}O$ and $(C_6H_5)_2Si{=}O$

Valery N. Khabashesku [a,b,*], Zoya A. Kerzina [b], Konstantin N. Kudin [b], Oleg M. Nefedov [b]

[a] *Department of Chemistry, Rice University, Houston, TX 77005-1892, USA*
[b] *Zelinsky Institute of Organic Chemistry, Russian Academy of Sciences, 47 Leniskii prospekt, Moscow, 117913, Russian Federation*

Received 4 January 1998

Abstract

Transient organic silanones $(CH_3O)_2Si{=}O$ (**3**) and $(C_6H_5)_2Si{=}O$ (**4**) were generated by vacuum pyrolysis from 3,3-dimethoxy-6-oxa-3-silabicyclo[3.1.0]hexane (**6**) and its 3,3-diphenyl derivative (**7**), respectively, and after being trapped in argon cryogenic matrices at 12 K directly studied by IR spectroscopy. Vibrational assignments in the observed IR spectra of **3** and **4** have been made by comparison with the density functional theory B3LYP/6-311G(d, p) calculated harmonic frequencies and infrared intensities for these molecules and for the other silanones, $H_2Si{=}O$ (**1**), $(CH_3)_2Si{=}O$ (**2**), and $CH_3(CH_3O)Si{=}O$ (**5**), studied earlier by matrix isolation techniques. The observed bands at 1247 cm^{-1} in **3** and at 1205 cm^{-1} in **4** were assigned to the Si=O stretching modes, which under the influence of the same substituents show the similar frequency shifts as ν (M=O) in ketones, phosphinoxides, and sulfoxides. Under the conditions of vacuum pyrolysis studied the diphenylsilanone **4** was found to be more thermodynamically stable than the dimethoxy derivative **3**, while the latter indicated a higher kinetic stability towards cyclooligomerization than the silanones **2** and **4**.

1. Introduction

The silicon analogues of ketones (silanones), $R_2Si{=}O$, are important intermediates in the combustion of silanes [1], chemical vapor deposition processes employing the oxidation of silicon-containing precursors in microelectronics industry [2], production of ceramic powders [3], and of silicone-based materials [4]. Silanones have been suggested as transient species in silicon thin film plasma deposition and etching technology [5]. Evidence for the formation of the Si=O reactive centers on the surface of mechanically activated quartz has been obtained [6]. The parent silanone, $H_2Si{=}O$ (**1**), is suggested to be of interest in interstellar chemistry [7]. The silanones are frequently expected to be formed in the high-temperature or photochemically induced transformations of the silicon–oxygen-containing compounds, where they have been chemically trapped [8]. New routes to generation of silanones in the liquid phase have recently been reviewed [9].

The high polarity of the Si=O π-bond, estimated by quantum chemical calculations [8,10–12], accounts for the extreme reactivity of silanones towards dimerization and trimerization, which proceed with no barrier, in contrast to their carbon analogues. For this reason the direct spectroscopic characterization of silanones as monomers was only achieved in the 1980s. The inorganic silanones $F_2Si{=}O$ and $Cl_2Si{=}O$ have been synthesized in cryogenic matrices and their IR spectra was recorded by Schnöckel [13,14]. Withnall and Andrews reported the IR bands for matrix-isolated silanone **1**, and of its hydroxy derivatives, $HO(H)Si{=}O$ and $(HO)_2Si{=}O$ [15]. The $H_2Si{=}O$ species has also been characterized in the gas phase by the chemiluminescent emission spectrum in the visible region by Glinski et al. [16], and recently, by its millimeter-wave rotational spectrum [17].

* Corresponding author. Tel.: +1 713 5278101; fax: +1 713 5238236.

0022-328X/98/$19.00
PII S0022-328X(98)00726-8

The first organic silanone studied directly by physicochemical methods was dimethylsilanone, $(CH_3)_2Si{=}O$ (**2**). In 1983 Arrington et al. [18] reported the generation of **2** for further IR studies by an in situ cryogenic matrix reaction of dimethylsilylene with O-atoms photochemically generated from several precursors, such as O_3, N_2O, and C_2H_4O. However, this approach provides extremely low yields of silanone, based on the observed tiny IR peak at 1204 cm^{-1} attributed to **2** in [18] and the recent results obtained by Almond [19] in attempt to reproduce these experiments. The higher yields, sufficient for the observation of the intense IR spectrum of **2** and its d_6-analogue, were produced by vacuum pyrolysis of 3,3-dimethyl-6-oxa-3-silabicyclo[3.1.0]hexane and its 1,5-dimethyl and 3,3-bis(trideuteromethyl) derivatives, respectively [20–23]. The observed strong band at 1210 cm^{-1} in the IR spectrum was assigned to the Si=O stretching mode in **2**. This was in excellent agreement with the later work of Withnall and Andrews [24], where **2** and also the methylsilanone, $CH_3(H)Si{=}O$, were generated by photooxidation of methylsilanes in argon matrices. The IR frequencies for the heavier organic silanones, such as $(CH_3O)_2Si{=}O$ (**3**) and $(C_6H_5)_2Si{=}O$ (**4**), were reported in our preliminary publication [25]. New UV and IR absorptions, appearing after photoirradiation of matrix-isolated dimethoxysilylene, $(CH_3O)_2Si$, were tentatively assigned to methyl(methoxy)silanone, $CH_3(CH_3O)Si{=}O$ (**5**), by Maier et al. [26].

In a recent study Gole and Dixon [27] have assigned a portion of the FTIR spectrum of an oxidized porous silicon to the Si=O stretch of a surface-bound silanone-based fluorofor groups, such as ROSi=O, where R is H, SiH_3, or hydrocarbon radical. In view of this work, and continued matrix isolation efforts in search of alternative routes to produce silanones for further UV and IR detection, discussed in [19], we report here our matrix isolation IR studies of organic radical substituted silanones **3** and **4**. The experimental data are supplemented by the density functional theory calculations providing a basis for comparative vibrational analysis of the spectra of the series of silanones **1**–**5**.

For the matrix IR detection the silanones **3** and **4** were generated by vacuum pyrolysis of 3,3-dimethoxy (**6**) and 3,3-diphenyl-6-oxa-3-silabicyclo[3.1.0]hexane (**7**). The choice of these compounds as a precursors rested on a proven successful utilization of their 3,3-dimethyl derivatives for the generation and matrix IR observation of dimethylsilanone **2** [20–23].

2. Experiment and calculations

2.1. General methods

^1H and ^{13}C-NMR spectra of **6** and **7** were recorded on Jeol FX 90 and Bruker WM-250 spectrometers. Mass spectral analyses were performed on a Varian MAT 311 and an AEI MS 902 instruments at 70 eV ionization energy. GC-MS analyses were done on a Finigan MAT Incos 50 spectrometer using an RSL-200 capillary column (0.25mm × 30 m).

2.2. Materials

2.2.1. 3,3-Dimethoxy-6-oxa-3-silabicyclo[3.1.0]hexane (6)

This precursor was synthesized in 54% yield by the epoxidation reaction of *p*-(methoxycarbonyl)perbenzoic acid with 1,1-dimethoxy-1-silacyclopent-3-ene, which was prepared in accordance with the described procedure [28]. After distillation, **6** was isolated as a colorless liquid, bp 113°C/90 Torr. According to GLC analysis the purity of **6** was higher than 98%. ^1H-NMR ($CDCl_3$, 250 MHz): δ 0.90 dd (2H, CH_2), 1.13 d (2H, CH_2), 3.36 m (2H, CH, $J = 1.1$ Hz), 3.46 s (3H, CH_3), 3.47 s (3H, CH_3). ^{13}C-NMR ($CDCl_3$, 250 MHz): δ 11.08 (CH_2), 50.51 (CH_3), 55.05 (CH). IR (Ar matrix, 12 K): 3010 (m), 2950 (s), 2919 (m), 2851 (s), 1506 (m), 1465 (m), 1457 (m), 1421 (vw), 1396 (w), 1388 (vw), 1355 (vw), 1327 (vw), 1238 (w), 1195 (vs), 1187 (s), 1105 (m), 1095 (vs), 1082 (s), 1078 (s), 1034 (m), 968 (w), 936 (m), 927 (m), 857 (sh), 841 (m), 829 (w), 811 (m), 791 (s), 744 (w), 663 (vw), 590 (m), 515 (vw), 503 (vw), 500 (vw) cm^{-1}. EIMS (70 eV): m/z (relative intensity) 160 (3), 159 (14, M–H), 145 (53, M–CH_3), 133 (19), 117 (100), 107 (28), 91 (68), 87 (42), 77 (34), 59 (74).

2.2.2. 3,3-Diphenyl-3-sila-6-oxabicyclo[3.1.0]hexane (7)

The precursor **7** was synthesized by the epoxidation of 1,1-diphenyl-1-silacyclopent-3-ene, prepared in 85% yield according to a known procedure [29]. After recrystallization from pentane the epoxide **7** was isolated in 94% yield with the purity higher than 98%. ^1H-NMR ($CDCl_3$, 250 MHz): δ 1.55 d (2H, CH_2, $J_{gem} = 16$ Hz), 1.85 d (2H, CH_2), 3.70 m (2H, > CH), 7.5 m (10H, Ph). ^{13}C-NMR ($CDCl_3$, 250 MHz): 27.95 (CH_2), 57.54 (CH), 127.54, 127.82, 129.34, 134.55, 135.0 (Ph). IR (Ar matrix, 12 K): 3137 (vw), 3094 (w), 3076 (m), 3060 (m), 3008 (m), 2941 (m), 2927 (m), 2861 (w), 1610 (m), 1573 (w), 1490 (w), 1434 (s), 1408 (w), 1401 (m), 1385 (m), 1340 (vw), 1240 (m), 1183 (vs), 1159 (w), 1120 (s), 1111 (s), 1073 (w), 1022 (m), 1000 (m), 965 (m), 935 (s), 923 (s), 824 (s), 811 (vs), 792 (s), 756 (w), 740 (s), 732 (m), 722 (vs), 700 (vs), 667 (w), 590 (s), 554 (vs), 467 (s), 462 (m), 432 (vs) cm^{-1}. EIMS (70 eV): m/z (relative intensity) 252 (10, M^+), 225 (26), 209 (71), 208 (58), 183 (100), 181 (66), 174 (64), 164 (55), 163 (48).

2.3. Vacuum pyrolysis-matrix isolation spectroscopy

The matrix isolation set-up used in present work was described elsewere [20–23]. The vapors of **6** and **7** were

passed through a resistively heated quartz pyrolyzer (5–8 mm internal diameter, 50–90 mm length), coupled to a vacuum shroud of the optical helium cryostat. The pressure and temperature in the pyrolysis zone were varied from 1 to 1×10^{-4} Torr and 500–950°C, respectively. The pyrolysis products were cocondensed at 12–14 K with a large excess of argon (1:1000) on the reflective copper plate, located at a distance of 50 mm from the pyrolyzer orifice. The copper plate was cooled with the help of a closed cycle CSW-208R refrigerator from Air Products. The matrices were analyzed with the LOMO IKS-24 infrared spectrometer in the range of 400–4000 cm^{-1} using the reflection of the infrared beam from the cold copper substrate surface.

The controlled warm-up experiments of deposited matrices to diffusion temperatures 35–45 K, imperative for identification of spectral absorptions of transient species, were carried out with the help of a built-in heater. The matrices from the pyrolyzate of **6** and **7** were also warmed up to room temperature under vacuum for collecting the final pyrolysis products into a liquid nitrogen cooled trap. The collected condensates were further examined by taking their IR spectra after redeposition into argon matrices at 12 K.

2.4. Calculations

The ground state optimized geometries for silanones **1**–**5** as well as their harmonic vibrational frequencies and infrared intensities were computed at the density functional B3LYP level of theory [30,31] with the 6-311G(d, p) basis set of triple-zeta quality [32]. The calculations were performed with the Gaussian 94 program package [33]. The vibrational analysis of the computed frequencies was carried out with the assistance of a vibration visualization package and also on the basis of potential energy distributions (PED) for normal vibrational modes. The force constants in internal coordinates for the silanones **3** and **4** were calculated from the B3LYP/6-311G(d, p) second derivative output values.

3. Results and discussion

3.1. IR spectra of pyrolysis products of epoxide (6)

In the IR spectrum of matrix-isolated pyrolysis products of (**6**), produced at temperature 800°C and pressure 5×10^{-4} Torr in the reactor zone (Fig. 2a), six new bands at 888, 1102, 1174, 1199, 1247, and 1471 cm^{-1} were observed along with the peaks of 1,3-butadiene [34] and those of unreacted precursor **6**, whose spectrum is given in Fig. 1. After matrix annealing from 12 to 40 K, a simultaneous decay of these six bands was observed, indicating that they all belong to a transient

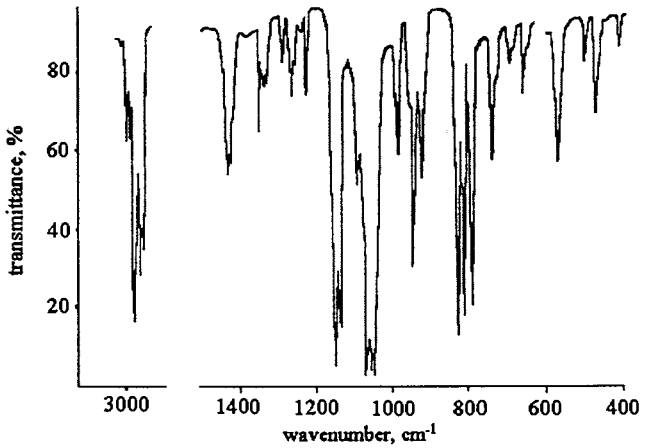

Fig. 1. IR spectrum of matrix-isolated (Ar, 12 K) 3,3-dimethoxy-6-oxa-3-silabicyclo[3.1.0]hexane (**6**).

species. The peaks in the 1050–1100 cm^{-1} spectral range and at 1450 cm^{-1}, characterizing the hexa(methoxy)cyclotrisiloxane, $[(CH_3O)_2SiO]_3$ (**8**), (denoted by MS-label) were observed to grow in the spectrum of the annealed matrix, while the band intensities of precursor (**6**) and butadiene remained virtually unchanged, as shown in Fig. 2b. When this matrix was warmed up to room temperature and the products were collected into a liquid N_2-cooled trap and then redeposited into an argon matrix, the IR spectrum of the new matrix did not exhibit any of the six bands.

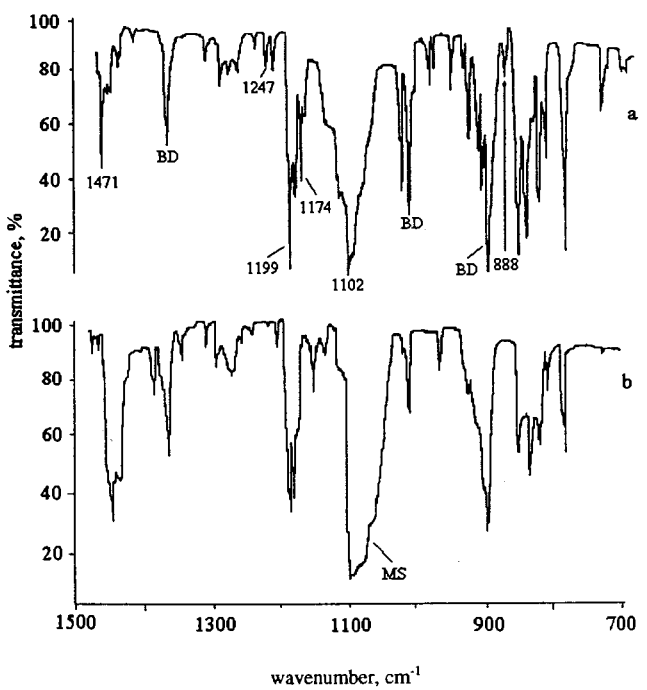

Fig. 2. IR spectra: (a) matrix-isolated (Ar, 12 K) pyrolysis (5×10^{-4} Torr, 800°C) products of **6**. (b) The matrix whose spectrum is shown under (b) after annealing from 12 to 40 K. Labels: BD, 1,3-butadiene; MS, methoxycyclosiloxanes **8** and **9**.

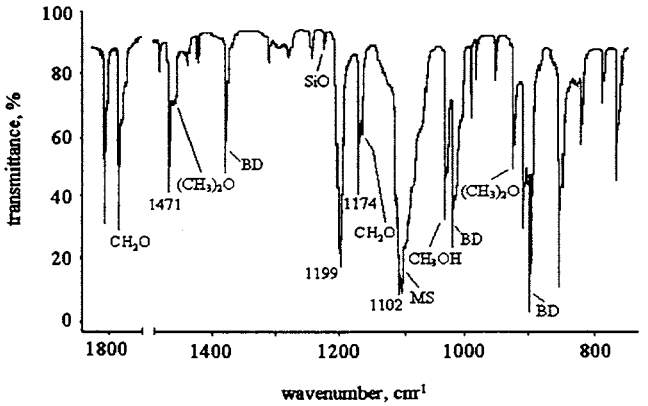

Fig. 3. IR spectrum (Ar, 12 K) of pyrolysis (10^{-1} Torr, 700°C) products of **6**. Labels: BD, 1,3-butadiene; MS-, methoxycyclosiloxanes **8** and **9**.

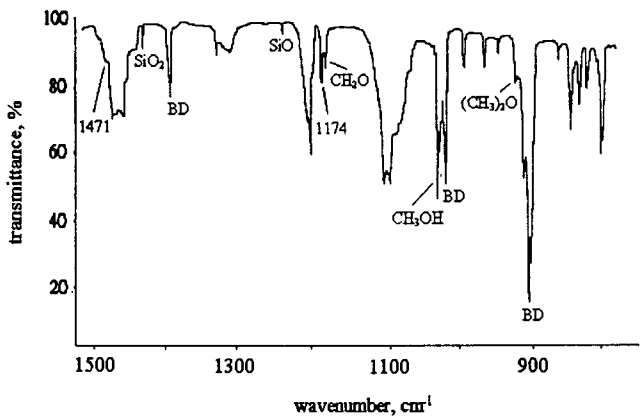

Fig. 4. IR spectrum (Ar, 12 K) of pyrolysis (10^{-3} Torr) products of **6** at elevated temperature of 930°C. Label: BD, 1,3-butadiene.

An increase of pressure in the pyrolysis zone from 5×10^{-4} to 10^{-1} Torr at the temperature 700°C, corresponding to a dramatic increase of the number of intermolecular collisions both in the gas phase and with the hot walls of the reactor, led to a notable weakening of the six new bands, growth of the peaks of tetra(methoxy)cyclodisiloxane, $[(CH_3O)_2SiO]_2$ (**9**), and trisiloxane **8**, and appearance of the absorptions of formaldehyde at 1748 cm^{-1} [35], methanol at 1035 cm^{-1} [36], dimethylether at 927 cm^{-1} [37], and of silicon monoxide at 1226 cm^{-1} [38] (Fig. 3). The latter small molecules along with the monomer silicon dioxide, exhibiting an absorption at 1419 cm^{-1} [39], were also identified in the spectrum of pyrolyzate produced from **6** at the elevated temperature (930°C) in the reaction zone (Fig. 4).

Taking into consideration the observed formation of butadiene as a 'leaving group' in the decomposition of epoxide **6** and the expected similarity of this reaction with the pyrolysis of 3,3-dimethyl analogue of **6**, which selectively led to the silanone, $(CH_3)_2Si{=}O$ (**2**) after elimination of butadiene [20–23], we believe that the new six bands can be assigned to the dimethoxysilanone **3**. This assignment allows to elucidate the accumulation of cyclosiloxanes either during matrix warm-up experiments or pressure increase in the reaction zone and agrees with the vacuum pyrolysis-MS studies of the decomposition of **6** [40]. The formation of smaller molecules at elevated pyrolysis temperatures can also be explained by a secondary process involving the silanone **3**, namely, the thermal dissociation according to Scheme 1. One more reason for the assignment of the six new IR features to the silanone **3** is also given by very good agreement between the observed and calculated frequencies and infrared intensities for **3** (Table 1).

3.2. IR spectra of matrix-isolated pyrolysis products of 3,3-diphenyl-6-oxa-3-silabicyclo[3.1.0]hexane (7)

In the spectrum of pyrolysis products of **7** at a temperature of 820°C and pressure of 1×10^{-2} Torr in the reactor (Fig. 6a), intense peaks of butadiene and new bands at 479, 541, 825, 1205 cm^{-1}, and the absorptions at 700, 1120, and 1205 cm^{-1}, have been observed along with a weak band of unreacted precursor **7**, whose spectrum is given in Fig. 5. Annealing of the matrix from 12 to 40 K brought about a remarkable change to the spectrum (Fig. 6b), namely, the depletion of all seven listed peaks with respect to absorptions of 1,3-butadiene and epoxide **7** and the

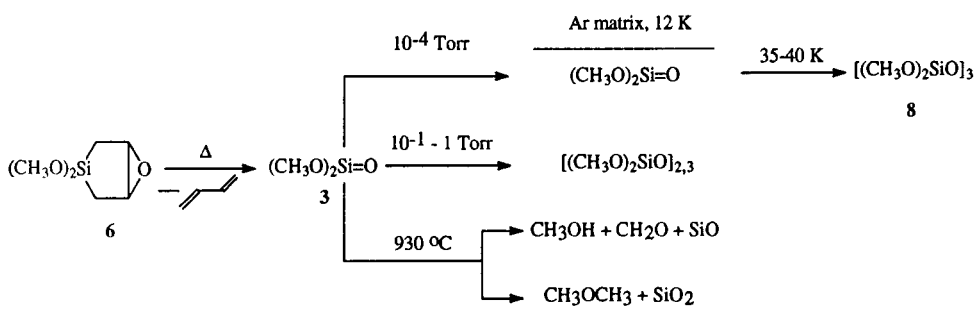

Scheme 1.

appearance of strong bands of hexaphenylcyclotrisiloxane, $[(C_6H_5)_2SiO]_3$ (**10**), identified by comparison with the IR spectrum (Fig. 7) of matrix-isolated authentic sample of **10**, synthesized exclusively for this purpose.

The new peaks at 479, 541, 825 and 1205 cm^{-1} were not observed in the spectrum of the pyrolyzate of **7** produced at the increased pressure of 10^{-1} Torr in the reactor, while the bands at 700, 1120 and 1434 cm^{-1}, overlapping with the peaks of precursor **7**, were observed to become weaker, and those of the trisiloxane **10** became more intense with respect to butadiene absorptions (Fig. 8). The increase of the pyrolysis temperature from 800 to 900–920°C at pressure 1×10^{-2} Torr in the reaction zone led to an observation in the spectrum, shown in Fig. 9, of seven weaker bands at 479, 541, 700, 825, 1120, 1205, and 1434 cm^{-1}, absorption of the SiO monomer at 1226 cm^{-1} [38], a strong band due to benzene at 675 cm^{-1} [41], and also a shoulder at 708 cm^{-1}, which very likely belongs to a phenyl radical [42].

The observed transformations of epoxide **7** and its pyrolysis products are summarized in Scheme 2. We are convinced that the most reasonable assignment of the observed seven new IR bands is to a monomer of diphenylsilanone **4**, which forms a cyclotrimer **10** either upon matrix warm-up or under increased pressure in the pyrolysis zone in a gas phase where possibly a transient cyclodimer of **4** is formed as well. The elevated temperatures in the pyrolysis zone result in dissociation of silanone **4** into SiO and phenyl radical along with benzene, that is likely to originate from a secondary bimolecular reaction. The proposed assignment also agrees with the calculations, that provide a good match of computed and observed frequencies for **4** (Table 2).

3.3. Thermal and kinetic stability of silanones

The silanones **3** and **4** were generated in the present work in the reactor of the same geometry as the one utilized previously for production of dimethylsilanone 2 [20–23]. This allows a qualitative comparison of the thermal and kinetic stability for the series of gas-phase generated silanones **2**–**4** by following the conditions (pressure and temperature) of their production as monomers and of their decay via secondary oligomerization or dissociation processes versus observed band intensities in the IR spectra. It was noted that unlike dimethyl- and diphenylsilanones, which get entirely oligomerized at the pressures of 10^{-1} Torr in the reactor, the dimethoxysilanone **2** under the same conditions still survives as a monomer, exhibiting its IR bands in the spectra. These data indicate a higher kinetic stability of the silanone **3** as compared to its dimethyl and diphenyl analogues, and also suggest that the kinetic stability of **3** is perhaps approaching that of dichlorosilanone, $Cl_2Si{=}O$, which was generated by the gas-phase pyrolysis and observed to survive as a monomer at pressures of about 1 Torr in the reactor, according to matrix isolation work of Golovkin et al. [43]. Based on ab initio studies of Kudo and Nagase [10], the dimerization of $H_2Si{=}O$ (**1**) is predicted to proceed with no barrier, which does not provide for an explanation of the observed differences in the kinetic stabilities of the larger molecules **2**–**4**. In our opinion, the latter can be related to the dipole moment change within the silanone monomer series, which at the same B3LYP/6-311G(d, p) level of theory are calculated to be the smallest in dimethoxysilanone, 1.97 Db, (Chart 1)

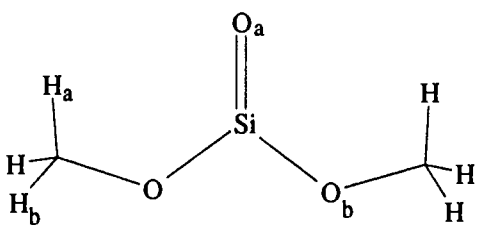

	bond distances (Å)					valence angles (deg.)					total atomic charges					dipole moment (Db)
	Si=O	Si-O	C-O	C-H_a	C-H_b	O_aSiO_b	$OSiO_b$	SiOC	H_aCO	H_bCO	Si	O_a	O_b	C	H	
HF/ 6-31G(d)	1.496	1.595	1.416	1.081	1.081	126.9	106.2	126.6	111.4	108.4	+1.38	-0.74	-0.70	-0.17	+0.18	2.32
B3LYP/ 6-31G(d)	1.527	1.624	1.438	1.094	1.094	127.8	104.4	123.3	111.8	108.3	+0.99	-0.57	-0.51	-0.21	+0.17	1.84
B3LYP/ 6-311G(d,p)	1.525	1.620	1.436	1.093	1.091	127.8	104.5	124.7	111.5	109.7	+1.16	-0.63	-0.55	-0.08	+0.12	1.97

and the largest, 4.87 Db, in diphenylsilanone (Chart 2)

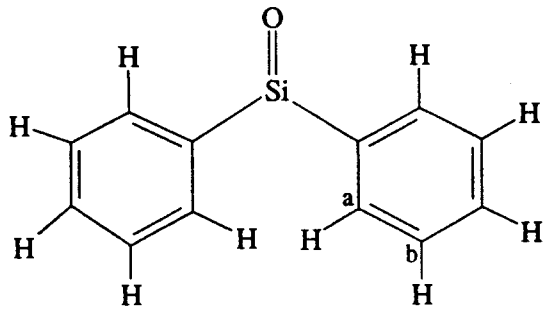

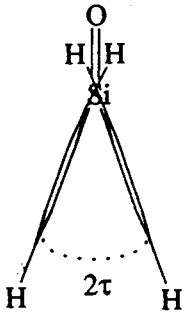

	bond distances (Å)					valence angles (deg.)							
	Si=O	Si-C	C-C_a	C_a-C_b	C-H	CSiO	CSiC	CCSi	C_aCC	CC_aC_b	HC_aC	HC_bC_a	τ
3-21G(d)	1.543[†]	1.850	1.410	1.395	1.083	122.5	114.9	122.9	118.4	120.8	119.8	120.0	25.9
	1.543[‡]	*1.853*	*1.407*	*1.395*	*1.082*	*119.2*	*121.7*	*127.5*	*118.2*	*120.9*	*120.5*	*119.9*	*0*
6-311G(d,p)	1.535[†]	1.858	1.406	1.391	1.084	121.6	116.8	123.9	118.6	120.6	120.2	119.9	23.7
	1.536[‡]	*1.861*	*1.405*	*1.392*	*1.082*	*119.1*	*121.7*	*127.5*	*118.3*	*120.8*	*120.8*	*119.8*	*0*

	total atomic charges[†]						dipole moment (Db)[†]
	Si	O	C	C_a	C_b	H	
3-21G(d)	+0.90	-0.43	-0.28	-0.18	-0.19	+0.20	4.43
6-311G(d,p)	+0.96	-0.59	-0.36	-0.06	-0.08	+0.11	4.87

[†] Given for the C_2 symmetry. [‡] Parameters for the C_{2v} symmetry are shown in italics.

and in dimethylsilanone, 4.61 Db (Fig. 10).

It was also found that the fragmentation of diphenylsilanone **4** proceeds at the same temperatures (900–920°C) in the reaction zone as the thermal destruction of dimethyl derivative **2**. This very likely indicates that the silanones **2** and **4** have similar thermodynamic stabilities, which at the same time are greater than that of dimethoxysilanone **3**.

3.4. Molecular geometries of silanones *1–5*

The B3LYP/6-311G(d, p) optimized structures and geometry parameters for the silanones **1**, **2**, and **5** are given on Fig. 10, while those calculated for diphenylsilanone **4** with the 3-21G(d) and 6-311G(d, p) basis sets at the same level of theory, and for the dimethoxysilanone **3** at the HF and DFT levels of theory, are shown on Charts 1 and 2. The calculations yielded structures with the lower symmetry (C_2) for diphenylsilanone **4** than for parent silanone **1**, dimethyl- and dimethoxysilanones, which were predicted to possess the C_{2v} symmetry. The planar structure with the C_{2v} symmetry for **4** was calculated to lie only by 1.14 kcal mol^{-1} at 3-21G(d), and 1.37 kcal mol^{-1} at 6-311G(d, p), higher in energy than the C_2 equilbrium geometry. However, computation of harmonic frequencies for the C_{2v} structure of **4** yielded a negative value for the frequency of the torsion mode of phenyl groups around the Si–C bonds and indicated that this structure characterizes a transition state. Thus, the reduction of the molecular symmetry in **4** is likely facilitated by the repulsion of *ortho*-hydrogen atoms of neighboring phenyl groups, causing their rotation around the Si–C bonds until the total energy minimum is reached at a dihedral angle τ, calculated to be 25.9 and 23.7° at B3LYP/3-21G(d) and 6-311G(d, p), respectively (Chart 2). The same twist around the C–C bond is found in the carbon analogue of **4**, $(C_6H_5)_2C{=}O$, giving a C_2

Table 1
Vibrations of dimethoxysilanone (**3**)

Mode	Symmetry	Frequencies (cm^{-1})				PED (%) and assignment
		HF/6-31G(d)[a]	B3LYP/6-31G(d)[b]	B3LYP/6-311G(d, p)[b]	Observed	
1	b_1	60(1)[c]	85(5)	85(6)[c]		94 COSiO symmetry in-plane bend
2	a_2	64(0)	89(0)	85(0)		100 CH_3 asymmetry torsion
3	b_1	83(7)	94(2)	91(1)		100 CH_3 symmetry torsion
4	a_1	125(7)	133(5)	128(6)		75 COSi symmetry in-plane bend; 25 OSiO scissor
5	a_2	137(0)	134(0)	140(0)		100 COSiO twist
6	b_2	172(37)	180(30)	169(32)		79 COSi asymmetry in-plane bend; 21 OSiO in-plane rock
7	a_1	334(15)	349(10)	346(10)		68 OSiO scissor; 32 COSi; symmetry in-plane bend
8	b_1	383(132)	350(65)	357(74)		98 OSiO wag
9	b_2	418(46)	417(24)	406(28)		77 OSiO in-plane rock; 22 COSi asymmetry in-plane bend
10	a_1	710(53)	724(39)	716(41)		87 Si-O symmetry str
11	b_2	835(33)	862(27)	848(25)	888(w)	62 Si-O asymmetry str; 38 C-O asym str
12	b_2	1103(847)	1119(654)	1108(654)	1102(vs)	74 C-O asymmetry str; 23 Si-O; asym str
13	a_1	1161(15)	1123(8)	1112(7)		93 C-O symmetry str
14	a_2	1172(0)	1194(0)	1180(0)		93 CH_3 rock ip
15	b_1	1175(5)	1198(0.4)	1184(0.1)		93 CH_3 rock op
16	a_1	1193(6)	1216(8)	1199(7)	1174(w)	75 CH_3 symmetry in-plane rock; 10 Si=O str
17	b_2	1205(193)	1231(118)	1213(138)	1199(s)	80 CH_3 asymmetry in-plane rock
18	a_1	1270(207)	1292(115)	1284(135)	1247(m)	95 Si=O str
19	b_2	1474(4)	1508(4)	1484(0.2)		100 CH_3 asymmetry deform
20	a_1	1480(2)	1514(0.1)	1490(0.1)		100 CH_3 symmetry deform
21	b_2	1489(0.1)	1530(1)	1501(1)		95 CH_3 asymmetry scissor deform
22	a_1	1490(4)	1531(9)	1501(13)	1471(w)	95 CH_3 symmetry scissor deform
23	a_2	1491(0)	1532(0)	1502(0)		87 CH_3 asymmetry scissor deform
24	b_1	1492(6)	1533(6)	1502(9)		87 CH_3 symmetry scissor deform
25	b_2	2913(102)	3060(103)	3036(101)		100 CH_3 asymmetry symmetry str
26	a_1	2915(0.1)	3062(0.1)	3037(0.1)		100 CH_3 symmetry symmetry str
27	b_2	2989(0.1)	3141(5)	3116(5)		100 CH_3 asymmetry asymmetry str
28	a_1	2990(75)	3142(28)	3116(30)		100 CH_3 symmetry asymmetry str
29	a_2	2991(8)	3143(0)	3117(0)		100 CH_3 asymmetry in-plane str
30	b_1	2992(45)	3144(51)	3117(53)		100 CH_3 symmetry in-plane str

[a] Scaled by 0.9.
[b] Unscaled.
[c] Intensity (km mol^{-1}).

structure instead of a C_{2v} structure. It should be noted that both geometries (C_2 and C_{2v}) in **4** reduce significantly the degree of π-conjugation of the Si=O double bond with the phenyl aromatic rings in **4**, which is reflected by the very small calculated Si–C bond shortening (0.011 Å) in **4** with respect to that in dimethylsilanone (Fig. 10). This contrasts with the earlier calculated significant shortening of the Si–C bond (by 0.036 Å) in the C=Si–C=C fragment of silacyclopenta-1,4-diene, for which spectroscopic evidence for strong π-conjugation has been obtained [44].

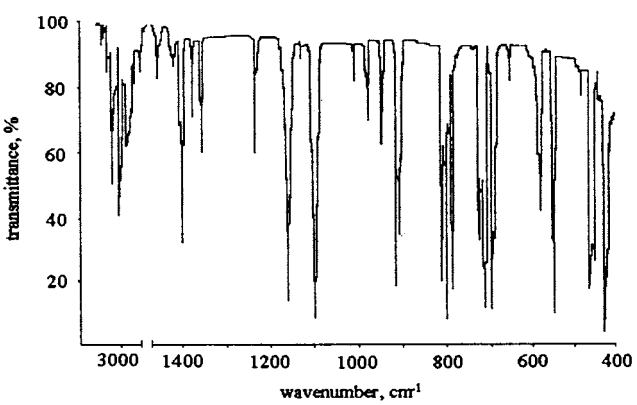

Fig. 5. IR spectrum of matrix-isolated (Ar, 12 K) 3,3-diphenyl-6-oxa-3-silabicyclo[3.1.0]hexane (**7**).

At the same (B3LYP) level of theory the Si=O bond lengths in all studied silanones are found to be almost identical, lying within 1.525–1.535 Å. For comparison, the HF/6-31G(d) method yields lower values for parent silanone **1**, 1.498 Å [10], and dimethoxysilanone, 1.496 Å (Chart 1). However, according to Mulliken population analysis the calculated total atomic charges on the π-bonded Si and O atoms vary significantly within the chosen series, depending on the electron donating or withdrawing nature of the substituents. This is clearly demonstrated by the increasing charge partition

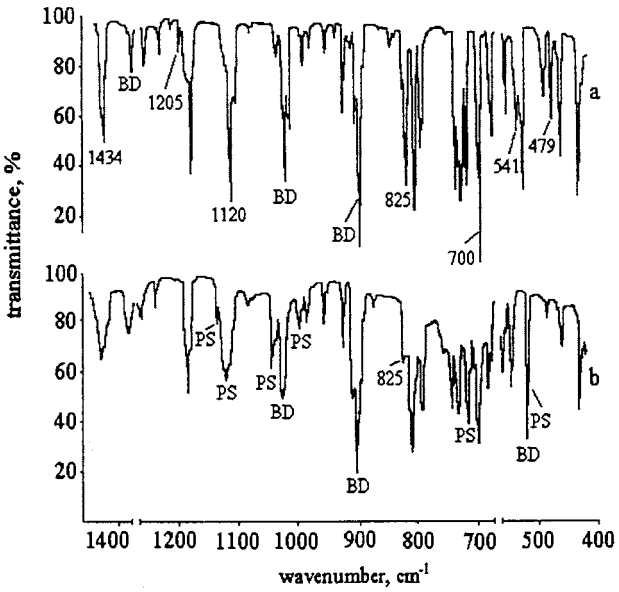

Fig. 6. IR spectra: (a) matrix-isolated (Ar, 12 K) pyrolysis (1×10^{-2} Torr, 820°C) products of **7**. (b) The matrix whose spectrum is shown under (b) after annealing from 12 to 40 K. Labels: BD, 1,3-butadiene; PS, hexaphenylcyclotrisiloxane **10**.

in the following direction: $H_2Si{=}O < (CH_3)_2Si{=}O < (C_6H_5)_2Si{=}O \approx CH_3(CH_3O)Si{=}O < (CH_3O)_2Si{=}O$. The B3LYP calculated dipole moments were found to change in the following order: $(C_6H_5)_2Si{=}O > (CH_3)_2Si{=}O > H_2Si{=}O \approx CH_3(CH_3O)Si{=}O > (CH_3O)_2Si{=}O$. The valence angles at the double-bonded silicon in **1**–**5** are calculated to be within 121.6–128.8°, thus confirming the sp^2 hybridization state of this atom.

3.5. IR spectra

A full assignment of IR bands of the silanones **3** and **4**, observed in the present work, and of those tentatively assigned to methyl(methoxy)silanone **5** in [26], has been suggested by comparison with the DFT calculated vibrational spectra for the whole series of silanones **1**–**5**, including the potential energy distributions (PED) for each vibrational mode. The high reli-

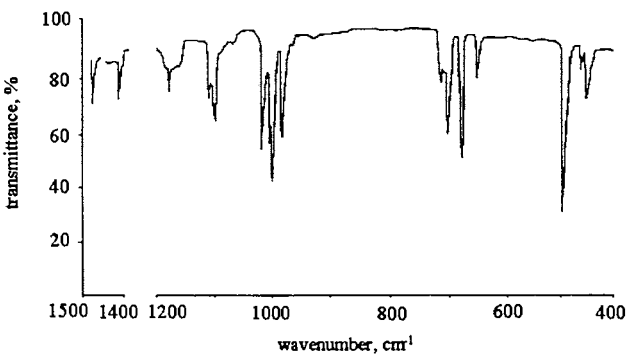

Fig. 7. IR spectrum of matrix-isolated (Ar, 12 K) hexaphenylcyclotrisiloxane (**10**).

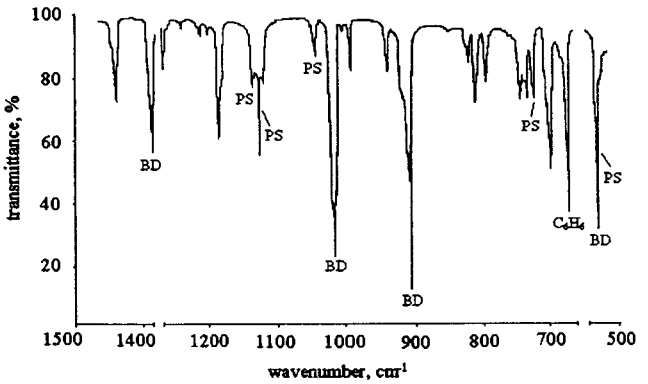

Fig. 8. IR spectrum (Ar, 12 K) of pyrolysis products of **7** at temperature 820°C and increased pressure (10^{-1} Torr) in the reactor. Labels: BD, 1,3-butadiene; PS, hexaphenylcyclotrisiloxane **10**.

ability of the B3LYP/6-311G(d, p) method in predicting the spectra of transient silenes, germenes, and germanones has already been demonstrated in our most recent studies [45]. In the present work we have extended the application of the same DFT method to vibrational analysis of the spectra of silanones.

In the Table 3 the frequencies for the $H_2Si{=}O$ molecule (**1**), previously calculated by the HF/6-31G(d) and SCF TZ2P(f, d) methods, are compared with the DFT spectral bands and infrared intensities computed in the present work, and with the experimental IR bands attributed to **1** by Andrews [15]. The unscaled DFT values are in much closer agreement with the experiment than the ab initio calculated frequencies [10], and confirm the vibrational assignment of the two yet observed bands in the spectrum of **1**, given earlier [15,46]. Therefore, we suggest that the DFT calculated data provide better guidance for further experimental detection of the other not yet observed spectral bands in **1**.

The DFT calculations done in present work also confirm the vibrational assignment of the observed bands in dimethylsilanone **2**, suggested in our previous

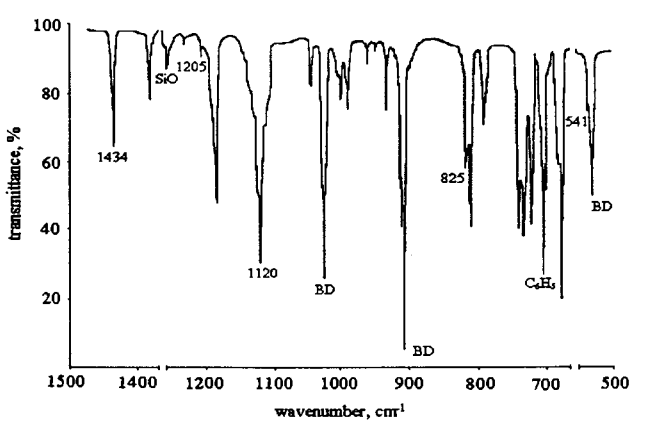

Fig. 9. IR spectrum (Ar, 12 K) of pyrolysis products of **7** at pressure of 1×10^{-2} Torr and elevated temperature of 920°C in the reactor. Label: BD, 1,3-butadiene.

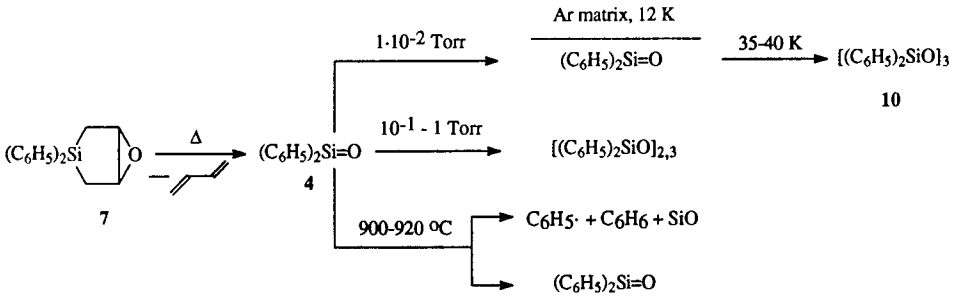

Scheme 2.

reports on basis of entirely empirical force field calculations [20–23]. The calculated and experimental frequencies for **2** and their assignment are presented in Table 4. The demonstrated excellent agreement between the theory and experiment in the case of silanones **1** and **2** encouraged the use of the DFT method for vibrational analysis of the observed spectra of the larger silanone molecules **3**–**5**.

The vibrational assignment for methyl(methoxy)silanone **5**, whose several IR bands have been reported by Maier et al. [26] is given in Table 5. The observed most intense feature at 1094.4 cm^{-1} is suggested to be attributed to the C–O stretching mode, in close agreement with the predicted value of 1103 cm^{-1} and the calculated highest intensity of this motion in **5**. To the CH_3(O) in-plane rocking mode we attributed an observed band at 1182.5 cm^{-1}, which agrees with the calculated frequency of 1199 cm^{-1}. The observed band at 1237.6 cm^{-1} is likely to belong to the Si=O stretching mode, according to the DFT predicted value of 1258 cm^{-1}, although one would expect a much higher intensity for the reported IR band in order to show a better agreement with the calculated infrared intensity of this mode in **5**. A possible way to solve this discrepancy will be to obtain an independent spectral data for **5** by using a different method for generation of silanone **5**. The other three observed bands at 1453.9, 2851.1, and 2981.0 cm^{-1} are attributed to the deformation mode of the CH_3 group attached to Si atom and to the symmetric and antisymmetric CH stretching vibrations of the CH_3 moiety attached to O atom, respectively, in agreement with calculated frequencies, vibration animation and PED values (Table 5).

The dimethoxysilanone molecule (**3**) of C_{2v} symmetry has 30 fundamentals, among which 19 vibrations are IR active in the 400–4000 cm^{-1} spectral region. We could observe six bands in the IR spectrum. The other bands are either of much lower intensity or overlapped by a strong absorptions due to the other molecules present in the matrix. In the Table 1 the frequencies of **3**, calculated with three different methods, are compared with the observed IR spectrum. The HF frequencies are scaled by a factor of 0.9 to allow better comparison with the experiment, while the B3LYP values are used without further scaling.

The observed weak band at 888 cm^{-1} was attributed to the antisymmetric Si–O stretching mode coupled with the antisymmetric C–O stretching mode, in agreement with the spectra calculations, PED values derived from the B3LYP/6-311G(d, p) output data, and vibration animation. The strongest observed band at 1102 cm^{-1} matches very well the calculated high intensity absorption of the antisymmetric C–O stretch coupled with the Si–O stretch of the same symmetry in **5**, which is predicted to lie within 1103–1119 cm^{-1} depending on the calculation method applied.

The CH_3 rocking modes of the CH_3O moiety in dimethyl(dimethoxy)silane, $(CH_3O)_2Si(CH_3)_2$ [47], as well as of the $C(CH_3)_2$ group in propane [41] are located in the 1145–1198 cm^{-1} IR spectral region. Therefore, we assigned an observed weak band at 1174 cm^{-1}, and a strong band at 1199 cm^{-1} to the symmetric and antisymmetric in-plane CH_3 rocking modes in **5**, respectively, in agreement with the calculations (Table 1). The observed weak band at 1471 cm^{-1} was attributed to the symmetric CH_3 scissoring deformation mode in **5** after comparison with the calculated frequency, PED and computer animation of this vibrational mode, and also after taking into account the literature data on IR spectra of dimethyl(methoxy) substituted silanes, where this mode is located in 1455–1465 cm^{-1} [47].

As to the Si=O stretching mode, the assignment of the observed medium intensity band at 1247 cm^{-1} in **3** was done on the basis of the well-documented spectral data which show an increase in the frequency of the M=O stretching mode in ketones, phosphinoxides, and sulfoxides on going from dimethyl to dimethoxy derivatives (Table 6). Our DFT calculations also predict the increase of the ν (Si=O) frequency under the influence of the CH_3O substituent in the silanones in the following direction: $(CH_3)_2Si{=}O$ (1227 cm^{-1}) < $CH_3(CH_3O)Si{=}O$ (1258 cm^{-1}) < $(CH_3O)_2Si{=}O$ (1284 cm^{-1}) (Tables 1, 4 and 5).

A DFT method also provides a cost-effective tool for computing the vibrational frequencies of larger

Table 2
Vibrations of diphenylsilanone (**4**)

Mode	Symmetry	Frequencies (cm^{-1})			PED (%) and assignment
		3-21G(d)[a]	6-311G(d, p)[a]	Observed	
1	b	32(1)	35(1)[b]		82 Ph torsion ip
2	a	41(0)	39(0)		64 Ph torsion op, 19 CSiO bend; 17 CCSi bend
3	a	80(0)	79(0)		75 CCSiO symmetry out-of-plane bend
4	b	100(3)	102(4)		67 CCCSi out-of-plane bend; 21 CCSi=O out-of-plane bend
5	b	141(9)	143(12)		87 CCSi asymmetry in-plane bend
6	a	167(0)	157(0)		90 CSiC twist
7	a	250(0)	239(0)		47 Si–C symmetry str, 34 CCC bend
8	b	263(15)	262(19)		82 CSiO in-plane bend; 11 Si–C asymmetry str
9	b	332(16)	326(18)		67 CSiO out-of-plane bend; 26 CCCC bend
10	a	381(2)	371(2)		40 CCSi symmetry in-plane bend, 20 CSiO; bend, 18 CCCC bend, 15 Si–C str
11	b	414(0)	405(0)		100 CCCC ring out-of-plane bend
12	a	424(0)	411(0)		100 CCCC ring out-of-plane bend
13	a	482(4)	463(3)		4 CCCC ring out-of-plane bend
14	b	491(40)	478(46)	479(m)	76 CCCC ring out-of-plane bend
15	b	513(130)	491(146)	541(s)	45 CCCC bend, 22 CSiO in-plane bend; 10 Si–C str
16	b	656(0)	631(0)		95 CCCC ring symmetry in-plane bend
17	a	658(0)	632(0)		95 CCCC ring symmetry in-plane bend
18	a	715(1)	693(1)		91 CCC ring in-plane bend
19	b	735(104)	715(70)	700(vs)	84 CCCC out-of-plane bend
20	a	742(13)	720(7)		87 CCCC out-of-plane bend
21	b	755(54)	736(63)		84 CCC bend, 16 Si–C asymmetry str
22	a	787(3)	758(6)		66 CCCC out-of-plane bend, 34 HCCC out-of-plane bend
23	b	787(29)	758(55)	825(s)	72 CCCC out-of-plane bend, 27 HCCC out-of-plane bend
24	b	892(2)	873(2)		100 HCCC out-of-plane bend
25	a	899(0)	879(0)		100 HCCC out-of-plane bend
26	b	974(2)	948(1)		92 HCCC out-of-plane bend
27	a	982(0)	956(0)		88 HCCC out-of-plane bend
28	b	1028(1)	998(1)		74 HCCC out-of-plane bend; 20 CCCC bend
29	a	1029(0)	1004(0)		80 HCCC out-of-plane bend, 18 CCCC bend
30	b	1030(12)	1013(7)		93 CCC bend
31	a	1035(0)	1015(0)		92 CCC bend
32	b	1054(0)	1021(0)		74 HCCC out-of-plane bend, 17 CCCC bend
33	a	1056(0)	1022(0)		60 HCCC out-of-plane bend, 30 CCCC bend
34	a	1066(10)	1046(1)		51 CC symmetry str, 25 CCC bend
35	b	1066(1)	1049(1)		56 CCC bend, 34 CC str
36	b	1107(0)	1096(1)		58 CC str, 14 HCC bend
37	a	1112(1)	1101(2)		41 CC str, 12 HCC in-plane bend; 11 CCC bend
38	a	1124(3)	1104(3)		86 CCC symmetry in-plane bend
39	b	1155(159)	1132(181)	1120(s)	82 CCC asymmetry in-plane bend, 12 Si–C asymmetry str
40	b	1235(0)	1186(0)		92 HCC asymmetry symmetry in-plane rock
41	a	1235(0)	1186(0)		90 HCC symmetry symmetry in-plane rock
42	b	1249(13)	1209(10)		100 HCC in-plane rock
43	a	1251(2)	1213(5)		88 HCC symmetry in-plane rock
44	a	1263(65)	1220(107)	1205(m)	99 Si=O str
45	b	1292(0)	1305(0)		74 CC asymmetry str
46	a	1298(4)	1311(4)		71 CC symmetry str
47	b	1387(6)	1354(3)		86 HCC asymmetry in-plane bend
48	a	1392(9)	1359(4)		88 HCC symmetry in-plane bend
49	b	1487(14)	1460(14)		80 HCC in-plane rock ip
50	a	1490(21)	1464(25)	1434(m)	78 HCC in-plane rock op
51	b	1540(1)	1514(0)		82 HCC symmetry in-plane rock ip
52	a	1542(3)	1514(0)		80 HCC symmetry in-plane rock op
53	b	1600(1)	1607(1)		41 CC asymmetry str, 33 CCC bend
54	a	1601(1)	1610(0)		42 CC symmetry str, 44 CCC bend
55	a	1619(7)	1630(8)		56 CC str
56	b	1620(13)	1630(18)		56 CC str
57	b	3193(2)	3166(1)		100 CH str
58	a	3195(0)	3167(0)		100 CH str
59	b	3198(1)	3173(1)		100 CH str

Table 2 (Continued)

Mode	Symmetry	Frequencies (cm^{-1})			PED (%) and assignment
		3-21G(d)[a]	6-311G(d, p)[a]	Observed	
60	a	3200(0)	3175(4)		
61	b	3206(7)	3180(12)		100 CH str
62	a	3207(1)	3182(2)		100 CH str
63	b	3215(14)	3188(14)		100 CH str
64	a	3216(21)	3189(21)		100 CH str
65	b	3226(29)	3195(36)		100 CH str
66	a	3226(6)	3196(10)		100 CH str

[a] B3LYP method.
[b] Intensity (km mol^{-1}).

molecules, in particular, diphenylsilanone **4**, and the assistance in vibrational assignment of the observed bands in **4**. The molecule **4** has 66 normal vibrational modes, among which 56 are predicted to be found in the 400–4000 cm^{-1} spectral region. We could observe seven bands, all located in the 400–1500 cm^{-1} region of the IR spectrum of matrix-isolated **4**. The rest of the bands, such as those of the =CH stretching modes, lying within 3000–3100 cm^{-1}, and of the other fundamentals, were not detected since they are either too weak or overlap the absorptions of the precursor **7** or 1,3-butadiene, present in the matrix.

The observed medium intensity band at 479 cm^{-1} was assigned to the phenyl ring out-of-plane bending mode in agreement with the calculated (Table 2) frequency (478–491 cm^{-1}) and intensity of this mode. A strong band at 541 cm^{-1} is attributed on basis of calculations, computer animation of vibrational modes and PED values to the phenyl ring bending mode coupled with the Si–C stretch and the CSiO in-plane bending vibration. The prominent peak, observed at 700 cm^{-1}, is suggested to belong to the ring out-of-plane CCCC bending mode. In the spectra of phenylsilanes the =CH out-of-plane bending mode is located in

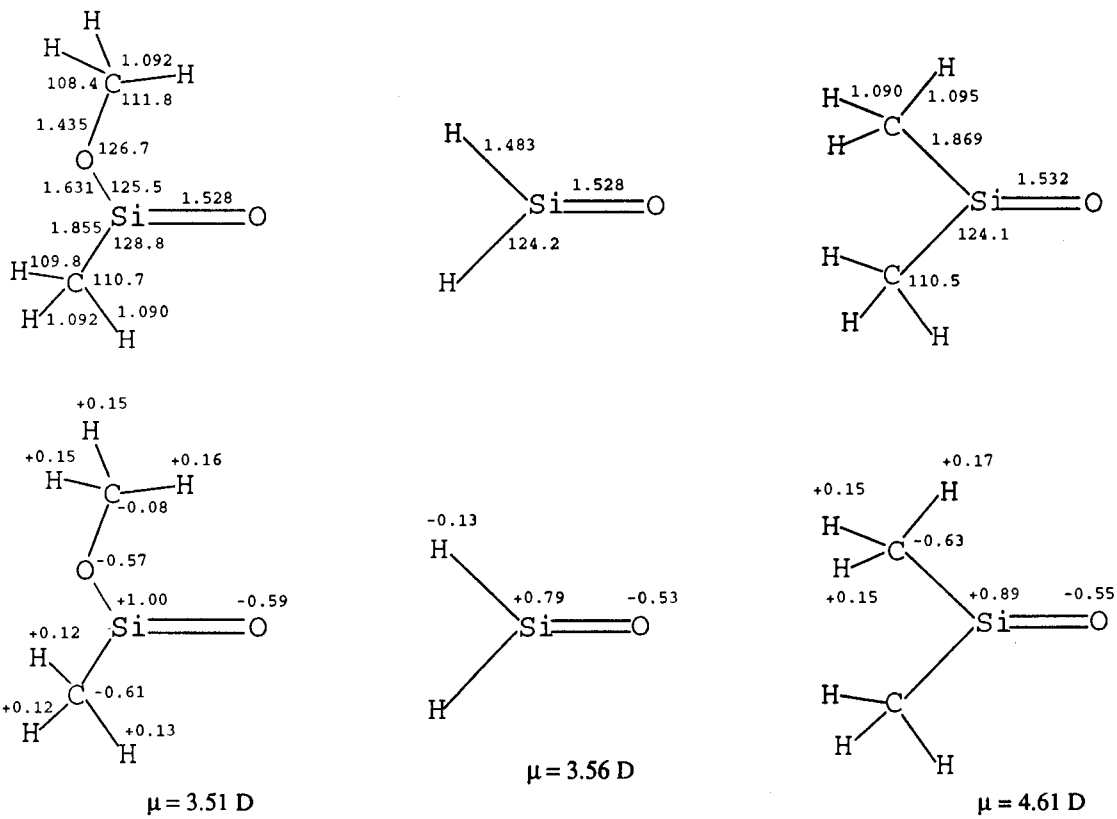

Fig. 10. Optimized B3LYP geometries of methyl(methoxy)silanone (**5**), parent silanone (**1**) and dimethylsilanone (**2**). Given are bond distances (Å), valence angles (°), atomic charges, and dipole moments (Db).

Table 3
Vibrations of silanone $H_2Si{=}O$ (**1**)

Mode	Symmetry	Frequencies (cm^{-1})			Observed	PED (%) and assignment[e]
		Reference [10][a]	Reference [45][b]	Present work[c]		
1	b_1	787	759	705(69)[f]	697	100 SiH_2 in-plane rock
2	b_2	812	802	710(66)		100 SiH_2 wag
3	a_1	1125	1080	1022(58)		100 SiH_2 scissor
4	a_1	1356	1356	1216(71)	1202	100 Si=O str
5	a_1	2432	2360	2229(45)		100 SiH_2 symmetry str
6	b_2	2433	2362	2245(164)		100 SiH_2 asymmetry str

[a] HF/6-31G(d).
[b] SCF TZ2P(f, d).
[c] B3LYP/6-311G(d, p).
[d] Reference [15].
[e] Present work
[f] Intensity (km mol^{-1}).

the 690–840 cm^{-1} [48]. The calculations predict this mode to be found in the silanone **4** at 758–787 cm^{-1} as a high intensity band and to be coupled with the ring out-of-plane CCCC motion (Table 2). The assignment of the observed strong band at 825 cm^{-1} to this vibration in **4** is in reasonable agreement with the considered above grounds. The CCC in-plane bending modes in phenylsilanes are found in the 1040–1130 cm^{-1} spectral region [48]. The calculations predict these modes in the silanone **4** also to be located in the same region (Table 4). Therefore, we assigned a strong band, observed at 1120 cm^{-1}, to this type of vibration. The detected band at 1434 cm^{-1} is attributed to the in-plane CH rocking mode in **4**, in reasonable agreement with the calculations.

Table 4
Vibrations of dimethylsilanone $(CH_3)_2Si{=}O$ (**2**)

Mode	Symmetry	Frequencies (cm^{-1})		PED (%) and assignment
		Calculated[a]	Observed	
1	a_2	26(0)[b]		100 CH_3 symmetry torsion
2	b_1	77(0.3)		100 CH_3 asymmetry torsion
3	a_1	223(0.02)		100 CSiC scissor
4	b_1	264(14)		100 SiC_2 wag
5	b_2	292(34)		100 SiC_2 in-plane rock
6	a_1	621(3)		100 Si–C symmetry str
7	b_2	686(10)	657(w)	85 Si–C asymmetry str
8	a_2	691(0)		96 CH_3 symmetry rock
9	b_1	800(32)	770(m)	86 CH_3 rock
10	b_2	810(128)	798(vs)	50 CH_3 asymmetry rock, 50 Si–C asymmetry str
11	a_1	863(22)	822(m)	81 CH_3 symmetry in-plane rock
12	a_1	1227(99)	1210(s)	100 Si=O str
13	b_2	1290(36)	1240(w)	100 CH_3 asymmetry deform rock
14	a_1	1296(48)	1244(m)	100 CH_3 symmetry deform rock
15	b_2	1446(2)		96 CH_3 deform
16	a_2	1450(0)		90 CH_3 deform
17	a_1	1457(4)		95 CH_3 deform
18	b_1	1466(22)		87 CH_3 deform
19	b_2	3023(0.3)		93 CH_3 str
20	a_1	3027(2)		93 CH_3 str
21	a_2	3085(0)		100 CH_3 str
22	b_1	3089(9)		100 CH_3 str
23	a_1	3130(2)		98 CH_3 str
24	b_2	3131(2)		98 CH_3 str

[a] B3LYP/6-311G(d, p).
[b] Intensity (km mol^{-1}).

Table 5
Vibrations of methyl(methoxy)silanone (5)

Mode	Symmetry	Frequencies (cm^{-1})		PED (%) and assignment
		Calculated[a]	Observed[b]	
1	a″	42(0)[c]		100 CH_3(Si) torsion
2	a″	72(0)		100 CH_3(O) torsion
3	a″	132(4)		96 COSiO out-of-plane bend
4	a′	148(16)		74 COSi, 26 OSiO in-plane bend
5	a′	243(12)		99 CSiO in-plane scissor
6	a″	304(37)		95 CSiOO out-of-plane bend
7	a′	397(34)		82 OSiO, 17 COSi in-plane scissor
8	a′	664(17)		84 Si–C, 13 Si–O str
9	a′	771(22)		49 Si–O, 24 C–O, 15 Si–C str
10	a″	781(23)		93 CH_3 out-of-plane rock
11	a′	861(70)		75 CH_3 in-plane rock
12	a′	1103(296)	1094.4 (1.00)	92 C–O str
13	a″	1181(0)		93 CH_3(O) out-of-plane rock
14	a′	1199(26)	1182.5 (0.26)	89 CH_3(O) in-plane rock
15	a′	1258(168)	1237.6 (0.09)	97 Si=O str
16	a′	1298(37)		99 CH_3 in-plane deform. rock
17	a′	1457(3)	1453.9 (0.13)	96 CH_3(Si) deformation
18	a″	1458(9)		89 CH_3(Si) deformation
19	a′	1483(1)		100 CH_3(O) deformation
20	a′	1500(8)		96 CH_3(O) deformation
21	a″	1503(5)		87 CH_3(O) deformation
22	a′	3033(53)	2851.1 (0.09)	100 CH_3O CH symmetry str
23	a′	3045(1)		100 CH_3Si CH symmetry str
24	a″	3110(30)	2981.0 (0.09)	100 CH_3O CH symmetry str
25	a′	3113(17)		100 CH_3O CH symmetry str
26	a″	3113(1)		100 CH_3Si CH symmetry str
27	a′	3146(2)		100 CH_3Si CH symmetry str

[a] B3LYP/6-311G(d, p).
[b] Intensity (km mol^{-1}).
[c] Tentatively assigned to **5** IR bands and their relative intensities, as given in ref. [26].

The observed medium intensity band at 1205 cm^{-1} is located in the Si=O stretching mode region (1200–1300 cm^{-1}), already identified for the other substituted silanones (Table 6). Besides that, the frequency of the Si=O stretch in **4** is expected to be shifted to a lower value relative to that in dimethyl derivative by analogy with the frequency change of the M=O (M=C, P, S) stretching mode in ketones, phosphinoxides, and sulfoxides (Table 6). This expectation also agrees with the B3LYP/6-311G(d, p) calculations predicting high intensities and a somewhat lower frequency value for **4** of C_2 symmetry (1220 cm^{-1}) as well as of C_{2v} planar geometry (1210 cm^{-1}) than for **2** (1227 cm^{-1}). Therefore, the assignment of the band at 1205 cm^{-1} to the Si=O stretching mode in **4** seems to have no alternative.

*3.6. The Si=O force constants and bond orders in silanones **1**–**5***

The calculated force constants of the Si=O bond in the internal coordinates for the silanones **1**–**5** are given in Table 7. They range within 8.5–9.0 mdyn $Å^{-1}$, exhibiting the highest value for dimethoxysilanone **3** (8.95 mdyn $Å^{-1}$) and the lowest for diphenyl substituted derivative **4** (8.59 mdyn $Å^{-1}$). They all notably exceed the force constant of the Si–O single bond, e. g. in $(CH_3)_3SiOCH_3$ (4.6 mdyn $Å^{-1}$) or in $(CH_3)_3SiOSi(CH_3)_3$ (5.3 mdyn $Å^{-1}$) [47], pointing out at a strong π-bonding between Si and O atoms in **1**–**5**. The Si=O force constant in dimethylsilanone **2**, 8.75 mdyn $Å^{-1}$, calculated in present work from B3LYP output data, is higher than our previously estimated value of 8.32 mdyn $Å^{-1}$ from the force field approximation [20–23]. Since molecular geometry is not optimized in this type of calculations, the latter force constant value seems now somewhat underestimated.

Application of an empirical Siebert's rule yielded the Si=O bond orders in **1**–**5**, lying within 1.65–1.72. Among the series studied these values indicate a higher π-bond order in dimethoxysilanone (1.712) and a lower degree of Si=O double-bonding in diphenylsilanone (1.658) than in the other silanones (Table 7). These bond orders are consistent with the Si=O frequency change in silanones 2–5, i. e. the higher bond order is related to the higher frequency. The bond order in parent silanone **1**, being higher than in **2**, but corre-

Table 6
Frequencies of the M=O (M=C, P, S, Si) stretching modes (cm^{-1}) in the IR spectra of selected ketones, phosphinoxides, sulfoxides, and silanones

	$(C_6H_5)_2C=O$	$(CH_3)_2C=O$	$(CH_3O)_2C=O$	$Cl_2C=O$	$F_2C=O$	Reference
C=O	1665	1719	1740	1823	1928	[41,51]
	$(C_6H_5)_3P=O$	$(CH_3)_3P=O$	$(CH_3O)_3P=O$	$Cl_3P=O$	$F_3P=O$	
P=O	1145	1161	1284	1292	1418	[49]
	$(C_6H_5)_2S=O$	$(CH_3)_2S=O$	$(CH_3O)_2S=O$	$Cl_2S=O$	$F_2S=O$	
S=O	1060	1103	1200	1251	1333	[50]
	$(C_6H_5)_2Si=O$	$(CH_3)_2Si=O$	$(CH_3O)_2Si=O$	$Cl_2Si=O$	$F_2Si=O$	
Si=O	1205	1210	1247	1240	1309	[13,14,20–23] and present work

Table 7
The calculated Si=O force constants (K) and bond orders (N) in silanones **1-5**

	$H_2Si=O$	$(CH_3)_2Si=O$	$CH_3O(CH_3)Si=O$	$(CH_3O)_2Si=O$	$(C_6H_5)_2Si=O$
K (Si=O) (mdyn $Å^{-1}$)	8.91	8.75 [8.32][b]	8.89	8.95	8.59
N (Si=O)	1.706	1.682 [1.45–1.53][a]	1.703	1.712	1.658

[a] Refs. [20–23].

sponding to a lower frequency of the Si=O stretch than in **2**, provides an exception from this trend. This deviation can be probably explained by the mixed nature of the Si=O stretching vibration, which in **1** is strongly coupled with the SiH_2 scissoring mode. This is indicated by the PED calculated values (Table 3) and computer animation of vibrational modes. Apart from that, all estimated bond orders in **1**–**5** seem to be in line with the B3LYP/6-311G(d, p) optimized Si=O bond lengths. This very likely conforms to the π-bond strengths, slightly increasing in **1-5** in the following direction: **4** < **2** < **5** ~ **1** < **3** (Charts 1 and 2, Fig. 10).

4. Conclusion

The vibrational analyses of the IR spectra of organic silanones **3** and **4**, generated in present work by vacuum pyrolysis of epoxides **6** and **7**, and of those for smaller molecules **1**, **2**, and **5**, observed in earlier studies [15,20–23,26], have been performed with the assistance of density functional theory calculations of harmonic frequencies and infrared intensities as well as computer animation and PED computation for each vibrational mode. The full descriptions of normal modes in **1**–**5** confirm the previous tentative spectral interpretation for **3** and **4** [23,25] and agree with the vibrational assignment for **1**, done on basis of HF calculations [10], and with that for **2**, suggested earlier by force field calculations [20–23].

The frequencies of the Si=O stretching modes in **1**–**5** all lie in the 1200–1300 cm^{-1} spectral region, as predicted by present DFT calculations, and are observed to increase under the influence of substituents in the following direction: $H_2Si=O < (C_6H_5)_2Si=O < (CH_3)_2Si=O < CH_3(CH_3O)Si=O < (CH_3O)_2Si=O$. The highest ν (Si=O) frequency value in the dimethoxysilanone **3** is in line with the strengthening of Si=O π-bond in this molecule due to a π-type electron donation from oxygen lone-pairs, which agrees with the observed enhanced kinetic stability of **3** towards cycloolygomerization as compared to the silanones **2** and **4**.

References

[1] (a) S. Fukutani, Y. Uodome, N. Kunoishi, H. Jinno, Bull. Chem. Soc. Jpn. 64 (1991) 2328. (b) J.R. Hartman, J. Famil-Ghirila, M.A. Ring, H.E. O'Neal, Combust. Flame 68 (1987) 43.
[2] (a) J.M. Jasinski, S.M. Gates, Acc. Chem. Res. 24 (1991) 9. (b) J.M. Jasinski, B.S. Meyerson, B.A. Scott, Ann. Rev. Phys. Chem. 38 (1987) 109. (c) K.F. Jensen, Adv. Chem. Ser. 22 (1989) 199.
[3] M.R. Zachariah, D. Chin, H.G. Semerjian, J.L. Katz, Combust. Flame 78 (1989) 287.
[4] D.R. Weyenberg, Silicones-past, present and future, in: E.R. Corey, J.Y. Corey, P.P. Gaspar (Eds.), Silicon Chemistry, Ellis Horwood, Chichester, 1988, pp. 285–296. (b) M.G. Voronkov, V.P. Mileshkevich, Yu. A. Yuzhelevskii, The Siloxane Bond, Consultants Bureau, New York, 1978.
[5] (a) G. Lukovsky, D. Tsu, R. Rudder, R. Markunas, Thin Film Processes II, in: J.L. Vossen, W. Kern (Eds.), Academic, Boston, 1991 pp. 565–619. (b) M.J. Kushner, J. Appl. Phys. 74 (1993) 6538.
[6] V.A. Radtsig, Khim. Fiz. 10 (1991) 1262 (Russian); C.A. 115: 240633v.
[7] J.L. Turner, A. Dalgarno, Astrophys. J. 213 (1977) 386.
[8] (a) G. Raabe, J. Michl, Chem. Revs. 85 (1985) 419. (b) G. Raabe, J. Michl, in: S. Patai, Z. Rappoport (Eds.), The Chemistry of Organic Silicon Compounds, Wiley, New York, 1989, pp. 1015.
[9] M.G. Voronkov, S. Basenko, J. Organomet. Chem. 500 (1995) 325.
[10] T. Kudo, S. Nagase, J. Phys. Chem. 88 (1984) 2833.
[11] (a) Y. Apeloig, Theoretical aspects of organosilicon compounds, in: S. Patai, Z. Rappoport (Eds.), The Chemistry of Organic

Silicon Compounds, vol. 1, Wiley, New York, 1989, pp. 57–225. (b) M.S. Gordon, Theoretical studies of multiple bonding to silicon, in: J.F. Liberman, A. Greenberg (Eds.), Molecular Structure and Energetics, vol. 1, VCH, Dierfield Beach, 1986, pp. 101–123.
[12] J. Kapp, M. Remko, P.V.R. Schleyer, J. Am. Chem. Soc. 118 (1996) 5745.
[13] H. Schnöckel, Z. Anorg, Allgem. Chem. 460 (1980) 37.
[14] H. Schnöckel, J. Mol. Struct. 65 (1980) 115.
[15] (a) R. Withnall, L. Andrews, J. Am. Chem. Soc. 107 (1985) 2567. (b) R. Withnall, L. Andrews, J. Phys. Chem. 89 (1985) 3261.
[16] R.J. Glinski, J.L. Gole, D.A. Dixon, J. Am. Chem. Soc. 107 (1985) 5891.
[17] S. Bailleux, M. Bogey, C. Demuynck, J.L. Destombes, A. Walters, J. Chem. Phys. 101 (1994) 2729.
[18] C.A. Arrington, R. West, J. Michl, J. Am. Chem. Soc. 105 (1983) 6176.
[19] M.J. Almond, Proceedings of the Second International Conference on Low Temperature Chemistry, Kansas City, August 4–9, 1996, pp. 117–120.
[20] (a) V.N. Khabashesku, Z.A. Kerzina, A.K. Maltsev, O.M. Nefedov, Izv. Akad. Nauk SSSR. Ser. Khim. (1986) 1215 (Russian). (b) V.N. Khabashesku, Z.A. Kerzina, A.K. Maltsev, O.M. Nefedov, Bull. Acad. Sci. USSR. Div. Chem., (1986) 1108 (England).
[21] A.K. Maltsev, V.N. Khabashesku, O.M. Nefedov, Low-temperature stabilization and direct spectroscopic study of intermediated with the Si=O multiple bonds, in: E.R. Corey, J.Y. Corey, P.P. Gaspar (Eds.), Silicon Chemistry, Ellis Horwood, Chichester, 1988, pp. 211–227.
[22] V.N. Khabashesku, Z.A. Kerzina, A.K. Maltsev, O.M. Nefedov, J. Organomet. Chem. 347 (1988) 277.
[23] Z.A. Kerzina, PhD Thesis, Zelinsky Institute of Organic Chemistry, Acad. Sci. USSR, 1989.
[24] R. Withnall, L. Andrews, J. Am. Chem. Soc. 108 (1986) 8118.
[25] (a) V.N. Khabashesku, Z.A. Kerzina, O.M. Nefedov, Izv. Akad. Nauk SSSR. Ser. Khim. (1988) 2187 (Russian). (b) V.N. Khabashesku, Z.A. Kerzina, O.M. Nefedov, Bull. Acad. Sci. USSR. Div. Chem. (1988) 1968 (England).
[26] G. Maier, H.P. Reisenauer, K. Schöttler, U. Wessolek-Kraus, J. Organomet. Chem. 366 (1989) 25.
[27] J.L. Gole, D.A. Dixon, J. Phys. Chem. B 101 (1997) 8098.
[28] E.A. Chernyshev, N.G. Komalenkova, S.A. Bashkirova, V.V. Sokolov, Zh. Obsh. Khim. 43 (1973) 785 Russian.
[29] S.T. Ioffe, A.N. Nesmeyanov, Methods of Organoelement Chemistry. Magnesium (Russian), Nauka, Moscow, 1963.
[30] J.M. Seminario, P. Politzer (Eds.), Modern Density Functional Theory: A Tool for Chemistry, Elsevier, Amsterdam, 1995.
[31] (a) A.D. Becke, J. Chem. Phys. 98 (1993) 5648. (b) C. Lee, W. Yang, R.G. Parr, Phys. Rev. B 37 (1988) 785.
[32] (a) R. Krishnan, J.S. Binkley, J.A. Pople, J. Chem. Phys. 72 (1980) 650. (b) A.D. McLean, G.S. Chandler, J. Chem. Phys. 72 (1980) 5639.(c) M.J. Frisch, J.A. Pople, J.S. Binkley, J. Chem. Phys. 80 (1984) 3265.
[33] (a) M.J. Frisch, G.W. Trucks, H.B. Schlegel, et al. GAUSSIAN 94, Gaussian Inc, Pittsburg, 1995.
[34] (a) P. Huber-Wülchli, Hs. H. Günthard, Spectrochim. Acta 37A (1981) 285. (b) J.J. Fisher, J. Michl, J. Am. Chem. Soc. 109 (1987) 1056. (c) B.R. Arnold, V. Balaji, J. Michl, J. Am. Chem. Soc. 112 (1990) 1808.
[35] K.B. Harvey, J.F. Ogilvie, Can. J. Chem. 40 (1962) 85.
[36] A.J. Barnes, H.E. Hallam, Trans. Farad. Soc. 66 (1970) 1920.
[37] G.P. Ayers, A.D.E. Pullin, Spectrochim. Acta 32A (1976) 1641.
[38] J.S. Anderson, J.S. Ogden, J. Chem. Phys. 51 (1969) 4189.
[39] H. Schnöckel, Angew. Chem. 90 (1978) 638.
[40] J. Tamas, A. Gomory, I. Beshenyei, V.N. Khabashesku, Z.A. Kerzina, N.D. Kagramanov, I.O. Bragilevsky, J. Organomet. Chem. 387 (1990) 147.
[41] L.M. Sverdlov, M.A. Kovner, E.P. Krainov, Vibrational Spectra of Polyatomic Molecules, Wiley, New York, 1973.
[42] (a) J.G. Radziszewski, M.R. Nimlos, P.R. Winter, G.B. Ellison, J. Am. Chem. Soc. 118 (1996) 7400. (b) J. Pacansky, D.W. Brown, J. Phys. Chem. 87 (1983) 1553.
[43] A. V. Golovkin, N. D. Mudrova, T. L. Krasnova, L. V. Serebrennikov, V. S. Nikitin, E. A. Chernyshev, Zh. Obshch. Khim., 55 (1985) 2802 (Russ.); (b) C.A. 104: 141052w.
[44] V.N. Khabashesku, V. Balaji, S.E. Boganov, et al., Mendeleev Comm. (1992) 38. (b) V.N. Khabashesku, V. Balaji, S.E. Boganov, O.M. Nefedov, J. Michl, J. Am. Chem. Soc. 116 (1994) 320.
[45] V.N. Khabashesku, K.N. Kudin, J.L. Margrave, J. Mol. Struct. 443 (1998) 175. (b) K.N. Kudin, J.L. Margrave, V.N. Khabashesku, J. Phys. Chem. B 102 (1998) 744. (c) V.N. Khabashesku, K.N. Kudin, J. Tamas, S.E. Boganov, J.L. Margrave, O.M. Nefedov, J. Am. Chem. Soc. 120 (1998) 5005. (d) V.N. Khabashesku, S.E. Boganov, K.N. Kudin, J.L. Margrave, O.M. Nefedov, Organometallics, submitted.
[46] B. Ma, H.F. Schaefer, J. Chem. Phys. 101 (1994) 2734.
[47] I.F. Kovalev, L.A. Ozolin, V.A. Arbuzov, I.V. Shevchenko, M.G. Voronkov, E. Ya. Lukevic, Izv. Akad. Nauk Latv. SSR (1970) 533.
[48] IR and UV spectra of phenylsilanes, in: Spectra and Chromatograms of Organoelement Compounds, Khimiya, Moscow, 1976.
[49] W.D. Burkhardt, E.G. Höhn, J. Goubeau, Z. Anorg, Allgem. Chem. 442 (1978) 19.
[50] D. Barton, U.D. Ollis, Phosphorus and sulfur compounds, Comprehensive Organic Chemistry, vol. vol. 5, Pergamon, New York, 1979.
[51] D. Lin-Vien, N.B. Colthup, W.G. Fateley, J.G. Grasselli, The Handbook of Infrared and Raman Characteristic Frequencies of Organic Molecules, Academic, San Diego, 1991.